# Quantum Stoner–Wohlfarth model of two-dimensional single-domain magnets

Essa M. Ibrahim ■ ; Shufeng Zhang



Journal of Applied Physics 133, 163901 (2023)

https://doi.org/10.1063/5.0143593





CrossMark

## Articles You May Be Interested In

Dynamic generalization of Stoner-Wohlfarth model

Journal of Applied Physics (June 2001)

New formulation of the Stoner-Wohlfarth hysteresis model and the identification problem

Journal of Applied Physics (May 1990)

Mathematica® code for Stoner-Wohlfarth processes

AIP Conference Proceedings (August 2012)





Cite as: J. Appl. Phys. 133, 163901 (2023); doi: 10.1063/5.0143593

Submitted: 24 January 2023 · Accepted: 3 April 2023 ·

Published Online: 24 April 2023









Department of Physics, University of Arizona, 1118 E 4th Street, Tucson, Arizona 85719, USA

<sup>a)</sup>Authors to whom correspondence should be addressed: essa@arizona.edu and zhangshu@arizona.edu

## **ABSTRACT**

The Stoner-Wohlfarth model is a classical model for magnetic hysteresis of single-domain magnets. For two-dimensional (2D) magnets at finite temperatures, the Stoner-Wohlfarth model must be extended to include intrinsic strong spin fluctuations. We predict several fundamentally different hysteresis properties between 2D and 3D magnets. The magnetization switching diagram known as the astroid figure in the conventional Stoner-Wohlfarth model becomes highly temperature dependent and asymmetric with respect to the transverse and longitudinal magnetic fields. Our results provide new insights into the spintronics applications based on 2D magnetic materials.

Published under an exclusive license by AIP Publishing. https://doi.org/10.1063/5.0143593

## I. INTRODUCTION

In the last several years, many two-dimensional (2D) magnetic materials with novel magnetic and spin transport phenomena have been discovered. 1-17 These new classes of 2D magnetic materials generate an interesting perspective for their possible applications in spintronics. To elucidate the fundamental differences between 2D and 3D magnets in response to an external magnetic field, we start with a single-domain magnet in which the magnetization is spatially uniform across the sample. The single-domain magnet is usually a building block for magnetic memory devices in which the direction of the magnetization can be well controlled by either the magnetic field or the electric currents. The most elementary magnetic property of a single domain is its very simple magnetic hysteresis described by the classical Stoner-Wohlfarth model, 1 whose magnetic energy is

$$E_{SW} = -K(\hat{\mathbf{z}} \cdot \mathbf{M})^2 - \mathbf{H} \cdot \mathbf{M}, \tag{1}$$

where M is the magnetization vector,  $\hat{\mathbf{z}}$  is the anisotropy axis with the anisotropy energy K, and  $\mathbf{H}$  is the applied magnetic field. For a single domain, the anisotropy constant K includes the crystal anisotropy and the demagnetization factor. The above simple Stoner-Wohlfarth model immediately gives rise to the well-known hysteresis loops for the different directions of the applied magnetic field, as shown in Figs. 1(a)-1(d). We note that an extension to the above single-domain model with an arbitrary anisotropic direction

would lead to more complicated hysteresis loops.<sup>20</sup>

In this paper, we study the magnetic hysteresis of two-dimensional single-domain magnetic particles with the uniaxial anisotropy, i.e., the 2D Stoner–Wohlfarth model. Why does the above successful Stoner–Wohlfarth model for the conventional 3D magnet fail for 2D magnets? In 3D, the magnitude of the magnetization,  $M_s(T) = |\mathbf{M}|$  is controlled by the exchange interaction between the neighboring spins, and, thus, it weakly depends on the magnetic field or the magnetic anisotropy as long as the temperature is not too close to the Curie temperature. Since the hysteresis of is measured with a constant temperature,  $M_s$  does not change for  $\frac{9}{43}$  the entire range of the field in the hysteresis. In 2D, however, the magnitude of the magnetization depends on both the exchange  $\frac{\omega}{2}$ interaction and the total effective field  $\mathbf{H}_t$  (the sum of the anisotropy and the applied field) even at low temperatures. To see this, we recall that, due to the divergence of the number of longwavelength spin waves of the isotropic Heisenberg model of the 2D magnet, the long-range order is absent without the external field. This is known as the Wagner and Mermin theorem.<sup>21</sup> The same divergence would occur for the anisotropic Heisenberg model if the magnitude of the applied magnetic field is equal to the anisotropy field but in the opposite direction of magnetization such that the spin wave gap becomes zero, and, therefore, the gapless spin waves destroy the long-range order in the anisotropic Heisenberg model as well. The difference between the isotropic Heisenberg model and

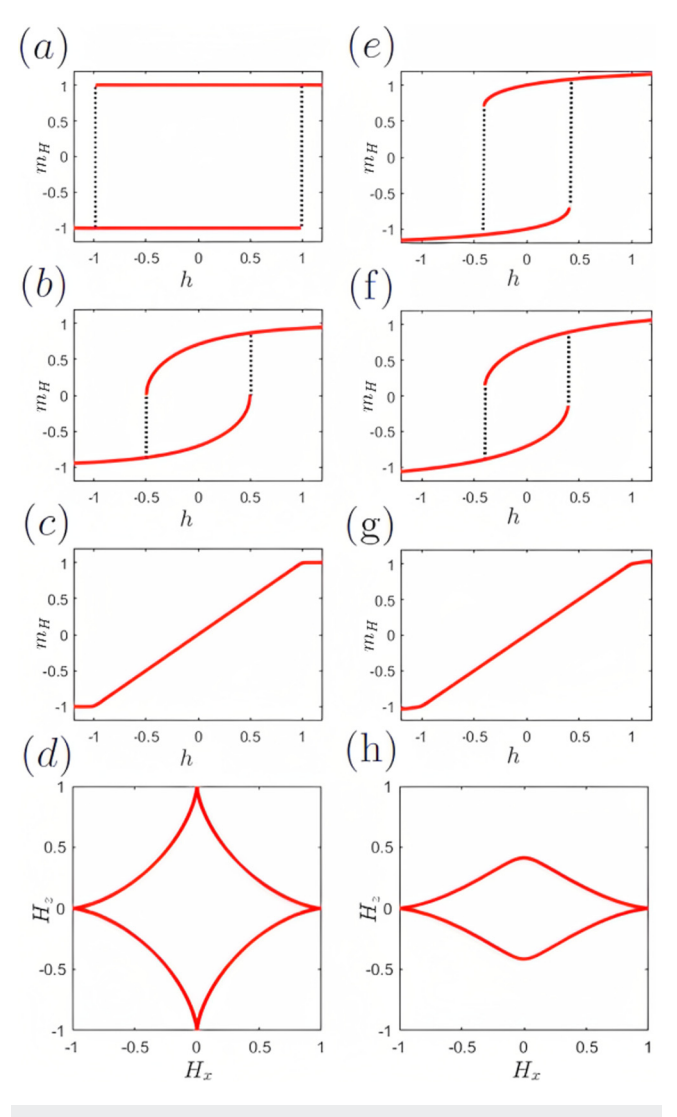


FIG. 1. Magnetic hysteresis and switching astroid for the 3D [four left panels (a)-(d)] and 2D [four right panels (e)-(h)] Stoner-Wohlfarth models. The magnitude of the magnetization is normalized by the magnetization at temperature T and at the zero field,  $M_0 = M(T, H = 0)$  for all figures, i.e.,  $m_H \equiv M_H/M_0$ , where  $M_H = \mathbf{M} \cdot \mathbf{H}/H$  is the magnetization in the direction of the magnetic field, which is normalized by 2K or 2zA and  $h \equiv H/2K$ . The hysteresis loops of a 3D magnet with the angles between the magnetic fields and the anisotropy axis: (a) at 0°, (b) at 45°, and (c) 90°. (d) The 3D astroid figure for magnetization switching fields. The hysteresis loops of the 2D magnet with the angles between the magnetic fields and the anisotropy axis: (e) at 0°, (f) at 45°, and (g) at 90° respectively. (h) The 2D astroid figure. All figures are calculated at the temperature  $T = 0.6T_c$ , where  $T_c$  is the Curie temperature.

the anisotropic Heisenberg model is that the induced magnetization instability occurs in all directions of the magnetization for the isotropic Heisenberg model, while for the anisotropic Heisenberg model, the disappearance of the magnetization occurs at one of the anisotropic orientations. In fact, after the spin waves destroy the long-range order, the magnetization would be spontaneously re-established in the direction parallel to the magnetic field. In this paper, we describe the variation of both magnitude and direction of the magnetization with the applied field by using the selfconsistent spin-wave method, which is equivalent to the random phase approximation. <sup>22</sup> In Figs. 1(e)–1(h), we show the 2D hysteresis alongside the conventional 3D hysteresis, followed by our detailed theory and calculation in Sec. II.

## II. MODEL

The quantum version of the 2D Stoner-Wohlfarth model with a uniaxial anisotropy (denoted as z-axis) is

$$\hat{\mathcal{H}} = -J \sum_{\langle i,j \rangle} \hat{\mathbf{S}}_i \cdot \hat{\mathbf{S}}_j - A \sum_{\langle i,j \rangle} \hat{S}_i^z \hat{S}_j^z - \sum_i \mathbf{H} \cdot \hat{\mathbf{S}}_i,$$
 (2)

where  $\hat{\mathbf{S}}_i$  and  $\hat{S}_i^z$ , respectively, are the spin and the z-component (taken as perpendicular to the two-dimensional plane) of the spin operators at lattice site  $\mathbf{R}_i$ , J is the isotropic exchange integral, A is the anisotropic exchange integral,  $\langle ij \rangle$  indicates the sum over nearest neighbors, and H is the external field. We use here natural units as we set  $\hbar = \mu_B = 1$ . In Eq. (2), we choose the exchange anisotropy rather than the single-site anisotropy since some 2D  $\frac{3}{5}$ magnets such as  $CrI_3$  have a dominant anisotropy from the exchange anisotropy;<sup>23</sup> this anisotropy exchange is equivalent to the anisotropy constant K = zA of Eq. (1), where z is the number of the nearest neighbor spins (z = 4 for a square lattice). To determine the magnetization, we have developed a random phase approximation (RPA) in which the transverse spin fluctuation and the longitudinal spin fluctuation are decoupled, and we have arrived at the self-consistent equation for the magnetization  $\frac{d^2k}{d^2k} = \frac{2M}{d^2k}$  (3) where  $M_s$  is the saturation magnetization at T = 0,  $\beta = (k_B T)^{-1}$ , and  $E_k$  is the magnon energy; in the long-wavelength limit,  $E_k = zM(2A + 0.5]k^2$ ) + H (assuming the field is along the direction of the anisotropy field). Equation (3) has a straightforward explanation: the magnetization is subtracted by the number of the magnons, which are softened by the factor of M at finite temperamagnets such as CrI<sub>3</sub> have a dominant anisotropy from the  $\frac{\dot{w}}{5}$ 

$$M = M_s - \int_{BZ} \frac{d^2k}{(2\pi)^2} \frac{2M}{e^{\beta E_k} - 1},$$
 (3)

magnons, which are softened by the factor of M at finite temperature. We note that (a) Eq. (3) is derived from the random phase  $\frac{1}{2}$ approximation for spin 1/2; the higher spins would lead to a more complicated equation; (b) compared to the conventional Holstein-Primakoff (HP) transformation, which is useful for low tempera-Primakoff (HP) transformation, which is useful for low temperatures, the random phase approximation neglects the correlation between the longitudinal and transverse spin fluctuation at different sites of the spins but retain all orders of other correlations.<sup>22</sup> The random phase approximation provides an excellent approximation for the equilibrium magnetization as long as the temperature is not too close to the Curie temperature. By using the quadratic dispersion for the magnon energy, we may integrate out  $d^2k$  in Eq. (3), resulting in a simpler analytical expression

$$M = M_s - \frac{1}{\pi z J} \left( \frac{1}{\beta} \ln \left| \frac{e^{\beta(\Delta + W)} - 1}{e^{\beta \Delta} - 1} \right| - W \right), \tag{4}$$

where  $\Delta = 2zAM + H$  and  $W = 2\pi zIM$  are the effective magnon gap and the magnon bandwidth, respectively. Since the quadratic dispersion of the magnon energy is used for the long-wavelength magnons, one may replace the entire magnon bandwidth W in Eq. (4) with a cutoff magnon energy. However, Eq. (4) is weakly dependent on W if  $\beta(\Delta + W) > 1$ ; thus, the choice of the cutoff energy is unimportant. Our hysteresis study will be based on Eq. (4): for a given temperature and a magnetic field, the magnitude of the magnetization is determined by Eq. (4) and the direction of the magnetization is parallel to the total effective magnetic field, which is the sum of the external field and the anisotropic field.

In order to make a direction comparison of the magnetic hysteresis between the Stoner-Wohlfarth model and ours, we need to properly renormalize the magnetization. In the classical Stoner-Wohlfarth model, the magnetization depends on temperature, but not the magnetic field. We, therefore, take the magnetization in our model at the zero magnetic field, the same as the classical one at a given temperature. In other words, we first solve Eq. (4) at a zero magnetic field to obtain  $M_0 = M(T, H = 0)$ . The hysteresis loops shown in Fig. 1 have the magnetization normalized by  $M_0$ .

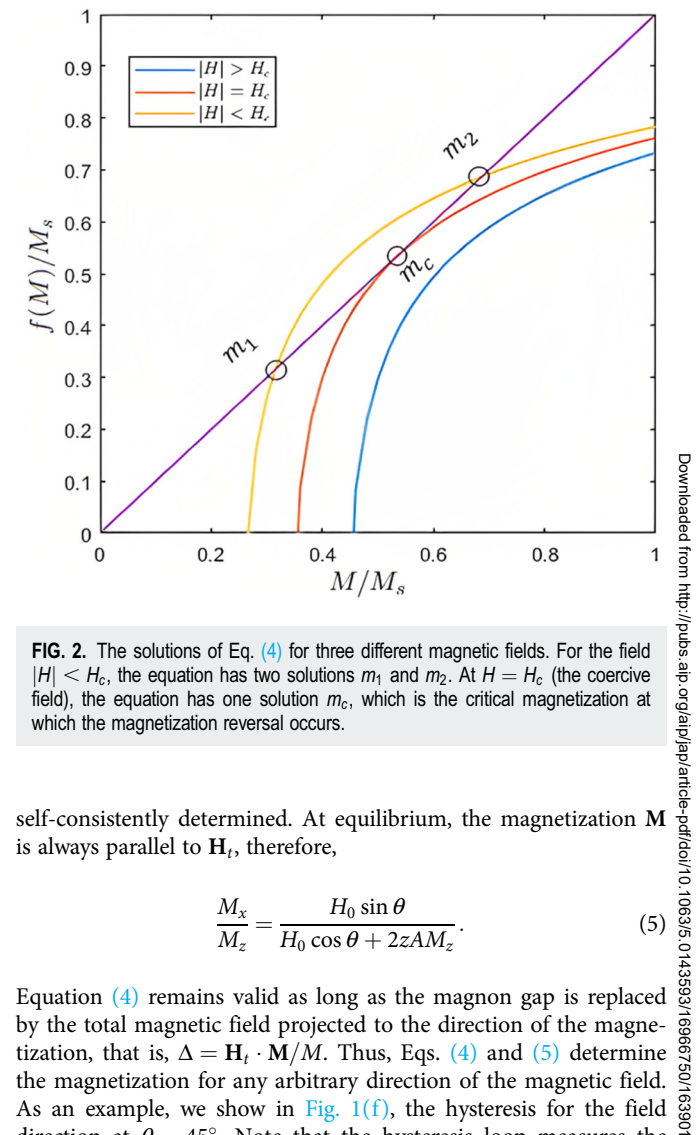
## III. EXTERNAL FIELD IN THE DIRECTION OF THE ANISOTROPY

The numerical solutions of M for the field in the direction of the anisotropy field are readily solved from Eq. (4). A simple way to obtain a solution for given parameters (temperature, field, and anisotropy) is to plot two functions y = M and y = f(M), where f(M) is the right side of Eq. (4). Note that the function f(M) is only physically meaningful when the magnon energy gap is positive, i.e.,  $\Delta > 0$ . The negative gap is unstable such that the magnetization reversal takes place. In Fig. 2, we show f(M) for three different magnetic fields: for a positive or small negative field, M = f(M) has two solutions, representing an energy minimum (the solution with a larger M) and an energy maximum. At a critical negative magnetic field, there is only one solution, which is also known as the coercive field. Beyond the critical field, there is no solution for M > 0, indicating magnetization reversal occurs.

Compared with the conventional Stoner-Wohlfarth model, the hysteresis shown in Fig. 1(e) is no longer square. The reduction of the magnetization near the critical value of the field is caused by the reduced effective gap and, thus, the increased number of magnons. Since the magnon population depends on the temperature, the magnetization at the critical magnetic field decreases significantly at higher temperatures as shown in Fig. 3. This contrasts with the 3D magnet, which is essentially independent of temperature.

## IV. EXTERNAL FIELD AT AN ARBITRARY DIRECTION

We now consider the hysteresis loop with the field in an arbitrary direction,  $\mathbf{H} = H_0(\hat{\mathbf{z}}\cos\theta + \hat{\mathbf{x}}\sin\theta)$ , where  $\theta$  is the angle between the applied field and the z-axis. The total effective field is the sum of the external and anisotropic field,  $\mathbf{H}_t = \mathbf{H} + 2zA(\mathbf{M} \cdot$  $\hat{\mathbf{z}}$ ) $\hat{\mathbf{z}}$ , where the direction and the magnitude of M need to be



$$\frac{M_x}{M_z} = \frac{H_0 \sin \theta}{H_0 \cos \theta + 2zAM_z}.$$
 (5)

As an example, we show in Fig. 1(f), the hysteresis for the field direction at  $\theta = 45^{\circ}$ . Note that the hysteresis loop measures the magnetization in the direction of the external field as a function of the magnetic field, namely, it is measuring  $m_h \equiv \mathbf{H} \cdot \mathbf{M}/|\mathbf{H}|$ . In the 3D Stoner–Wohlfarth model of Eq. (1), one can easily show that  $45^{\circ}$  is a special case where the magnetization along the direction of  $\frac{\omega}{8}$ the field is precisely zero at the coercive field, see Fig. 1(b). In 2D, the magnetization remains finite just below the coercive field as shown in Fig. 1(f) since the reversal occurs before the magnetization becomes zero. For  $\theta=90^\circ$  (the hard axis loops), both 2D and 3D hysteresis are single-valued. However, the 2D Stoner-Wohlfarth model has a non-zero slope even above the anisotropy field while the 3D Stoner-Wohlfarth model would be completely saturated above the anisotropy field.

We next construct the critical values of the magnetic field for the magnetization reversal for all directions of the magnetic field, known as the astroid figure. When the magnetic field increases across the astroid line, the reversal occurs. In the classical

Stoner–Wohlfarth model, the astroid line can be readily derived from Eq. (1), and the analytic expression of the astroid is  $H_z^{2/3} + H_x^{2/3} = (2K)^{2/3}$ . In the 2D Stoner–Wohlfarth model, the astroid is highly temperature dependent as shown in Fig. 4. At low temperatures, the astroid figure resembles that of the 3D Stoner–Wohlfarth model. At higher temperatures, the magnetization reversal for the longitudinal field (parallel to the anisotropy field) is more effective than for the transverse field. This is because, for the same magnitude of the field, the longitudinal direction reduces the magnon gap more than the transverse direction, leading to the asymmetry of the astroid figure in the

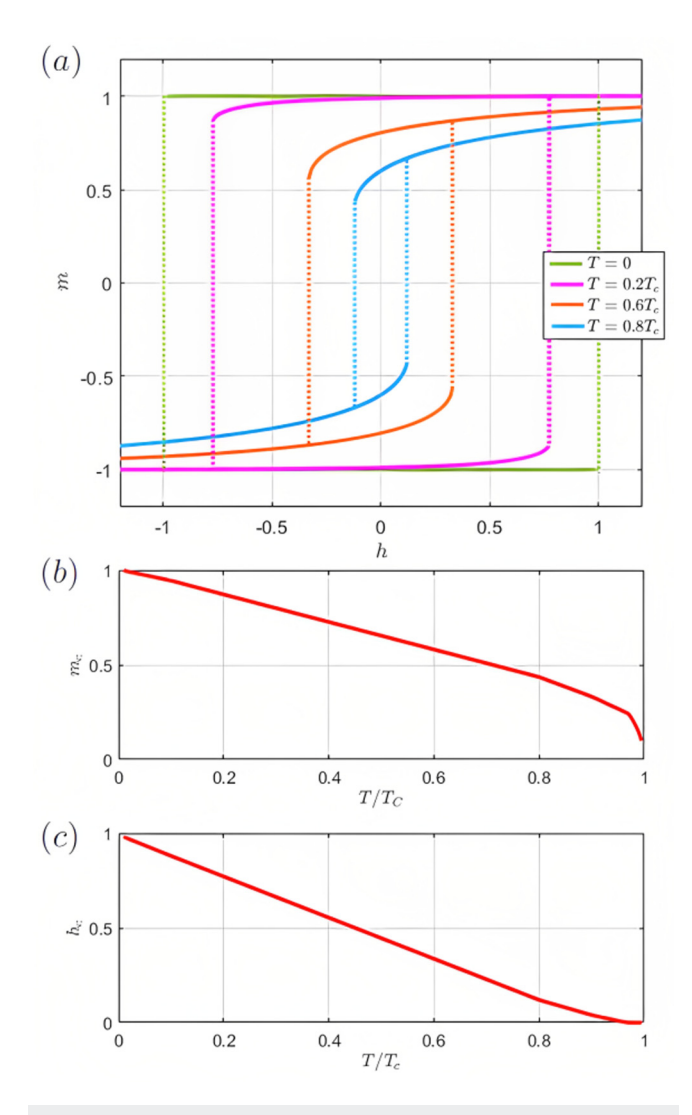


**FIG. 3.** (a) The hysteresis of a single-domain 2D magnet at different temperatures (magnetization is normalized at zero temperature  $M_{\rm s}$ ) with the field parallel to the anisotropic axis. (b) The temperature dependence of the critical magnetization. (c) The temperature dependence of the coercive field.

direction of the applied field (loss of the fourth-order symmetry of the astroid curve).

#### V. EFFECTS OF FINITE SAMPLE SIZE

Up until now, we have only considered an infinite size of the single-domain magnet in which the long-wavelength magnons are responsible for the strong spin fluctuation. For a large magnet, the switching of the magnetization is, in general, through domain wall nucleation and propagation due to the presence of magnetic impurities and boundary roughness. Therefore, the single-domain assumption is only experimentally meaningful for a small magnet. To see how the finite size changes, our calculation and what the minimum size needed to observe the predicted hysteresis loops, we may introduce a maximum wavelength of the magnon spectrum to be the size of the sample  $L_m$ , or equivalently, a cutoff minimum wave vector  $k_{\min} = 2\pi/L_m$  such that the integral of Eq. (3) has the range from  $k_{\min}$  to the bandwidth W. Consequently, the effective gap in Eq. (4) becomes  $\Delta = zM(2A + 0.5)k_{\min}^2 + H$ .

To estimate how the additional gap  $0.5zMJk_{\min}^2$  induced by the finite size affects the hysteresis, one may identify the coercivity  $H_c$  in Fig. 1(e) is shifted by  $0.5zMJk_{\min}^2$  toward the classical value of 2zMA. If  $0.5Jk_{\min} \ll A$ , or equivalently, the sample size  $L_m \gg \pi \sqrt{J/A}$  in units of the lattice constant, the correction of the finite size becomes insignificant. Recall that  $\pi \sqrt{J/A}$  is the domain wall width, which is only about several nanometers if A is two orders of magnitude smaller than J. Thus, as long as the single domain can be maintained at a size larger than the domain wall width in experiments, our calculations remain valid.

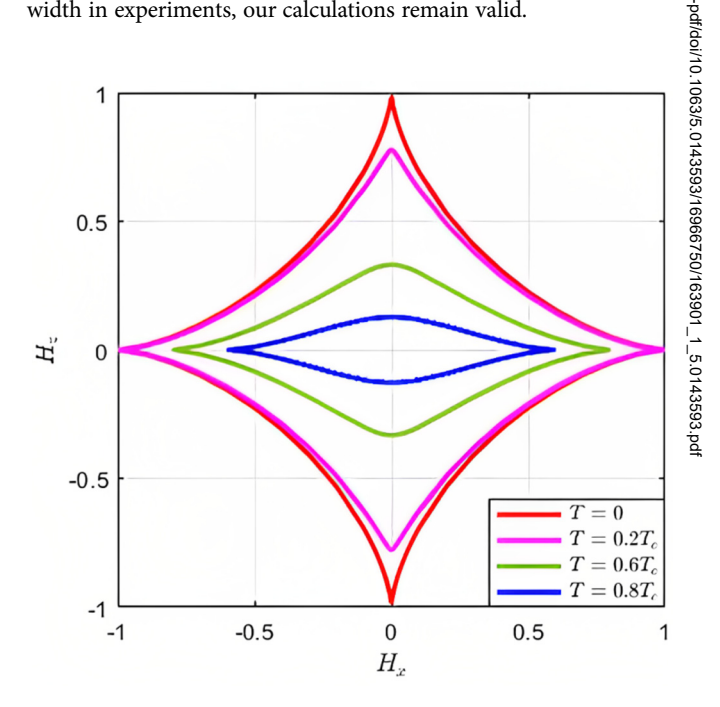


**FIG. 4.** The temperature dependence of the astroid diagram for a 2D single-domain magnet ( $2zAM_s = 1$ ).

#### VI. SUMMARY AND CONCLUSIONS

Due to the fundamentally strong spin fluctuation of 2D magnets, the classical Stoner–Wohlfarth model, which is widely used for modeling elementary hysteresis of a uniaxial anisotropic 3D magnet fails to account for the external field dependence of magnetization. By using our previously established random phase approximation for the equilibrium magnetization of the 2D magnet, we find that (1) the hysteresis involves the magnetization collapse at a critical field such that the long-range order is destroyed by the spin wave excitations, (2) the coercivity is significantly smaller than that of the 3D magnet for the same anisotropic constant, (3) the fourth-order symmetry of the astroid curve is lost, and (4) the above behavior is more pronounced at higher temperatures.

Finally, we comment on the current experimental status of the 2D single-domain hysteresis. The direct comparison of the singledomain model of the 2D magnet with experiments is difficult at the present time due to non-single 'domain hysteresis. In experiments, hysteresis is measured in a film with a large lateral size, for example, the hysteresis loops of high-quality CrBr3 monolayers have been experimentally measured by photoluminescence,<sup>24</sup> and it is certain that the film breaks up into domains in various stages of the hysteresis. The physical origins of the domain wall formation could be intrinsic such as long-range dipolar interactions and edge effects or could be extrinsic such as film roughness or impurities. To account for these experimental complications, one needs to develop new micromagnetic theories, including the change of the magnetization amplitude during the hysteretic processes, that can be broadly used for the 2D magnet with the spin fluctuations included.

## **ACKNOWLEDGMENTS**

This work was partially supported by the U.S. National Science Foundation under Grant No. ECCS-2011331.

## **AUTHOR DECLARATIONS**

## Conflict of Interest

The authors have no conflicts to disclose.

#### **Author Contributions**

Essa M. Ibrahim: Conceptualization (supporting); Formal analysis (lead); Investigation (lead); Methodology (lead); Project administration (supporting); Resources (supporting); Software (lead); Validation (equal); Visualization (lead); Writing – original draft (supporting); Writing – review & editing (equal). Shufeng Zhang: Conceptualization (lead); Formal analysis (supporting); Funding acquisition (lead); Investigation (supporting); Project administration (lead); Resources (lead); Supervision (lead); Validation (equal); Writing – original draft (lead); Writing – review & editing (equal).

## DATA AVAILABILITY

Data sharing is not applicable to this article as no new data were created or analyzed in this study.

#### **REFERENCES**

- <sup>1</sup>B. Huang, G. Clark, E. Navarro-Moratalla, D. R. Klein, R. Cheng, K. L. Seyler, D. Zhong, E. Schmidgall, M. A. McGuire, D. H. Cobden, and W. Yao, "Layer-dependent ferromagnetism in a van der Waals crystal down to the monolayer limit," Nature **546**, 270 (2017).
- <sup>2</sup>C. Gong, L. Li, Z. Li, H. Ji, A. Stern, Y. Xia, T. Cao, W. Bao, C. Wang, Y. Wang, and Z. Q. Qiu, "Discovery of intrinsic ferromagnetism in two-dimensional van der Waals crystals," Nature 546, 265–269 (2017).
- <sup>3</sup>D. J. O'Hara, T. Zhu, A. H. Trout, A. S. Ahmed, Y. K. Luo, C. H. Lee, M. R. Brenner, S. Rajan, J. A. Gupta, D. W. McComb, and R. K. Kawakami, "Room temperature intrinsic ferromagnetism in epitaxial manganese selenide films in the monolayer limit," Nano Lett. 18, 3125 (2018).
- <sup>4</sup>D. R. Klein, D. MacNeill, J. L. Lado, D. Soriano, E. Navarro-Moratalla, K. Watanabe, T. Taniguchi, S. Manni, P. Canfield, J. Fernández-Rossier, and P. Jarillo-Herrero, "Probing magnetism in 2D van der Waals crystalline insulators via electron tunneling," Science 360, 1218 (2018).
- <sup>5</sup>S. Jiang, L. Li, Z. Wang, K. F. Mak, and J. Shan, "Controlling magnetism in 2D CrI<sub>3</sub> by electrostatic doping," Nat. Nanotechnol. **13**, 549 (2018).
- <sup>6</sup>J. U. Lee, S. Lee, J. H. Ryoo, S. Kang, T. Y. Kim, P. Kim, C. H. Park, J. G. Park, and H. Cheong, "Ising-type magnetic ordering in atomically thin FePS<sub>3</sub>," Nano Lett. 16, 7433–7438 (2016).
- <sup>7</sup>B. Huang, M. A. McGuire, A. F. May, D. Xiao, P. Jarillo-Herrero, and X. Xu, "Emergent phenomena and proximity effects in two-dimensional magnets and heterostructures," Nat. Mater. 19, 1276 (2020).
- <sup>8</sup>C. Gong and X. Zhang, "Two-dimensional magnetic crystals and emergent heterostructure devices," Science 363, 4450 (2019).
- <sup>9</sup>T. Song, X. Cai, M. W. Y. Tu, X. Zhang, B. Huang, N. P. Wilson, K. L. Seyler, of L. Zhu, T. Taniguchi, K. Watanabe, and M. A. McGuire, "Giant tunneling mag netoresistance in spin-filter van der Waals heterostructures," Science 360, 201214–1218 (2018).
- 10 V. Gupta, T. M. Cham, G. M. Stiehl, A. Bose, J. A. Mittelstaedt, K. Kang, S. Jiang, K. F. Mak, J. Shan, R. A. Buhrman, and D. C. Ralph, "Manipulation of the van der Waals magnet Cr<sub>2</sub>Ge<sub>2</sub>Te<sub>6</sub> by spin-orbit torques," Nano Lett. 20, 7482 (2020)
- 11 D. MacNeill, G. M. Stiehl, M. H. D. Guimaraes, R. A. Buhrman, J. Park, and D. C. Ralph, "Control of spin-orbit torques through crystal symmetry in WTe<sub>2</sub>/ ferromagnet bilayers," Nat. Phys. 13, 300 (2017).
- 12M. Alghamdi, M. Lohmann, J. Li, P. R. Jothi, Q. Shao, M. Aldosary, T. Su, B. P. Fokwa, and J. Shi, "Highly efficient spin-orbit torque and switching of layered ferromagnet Fe<sub>3</sub>GeTe<sub>2</sub>," Nano Lett. 10, 4400 (2019).
- 13X. Wang, J. Tang, X. Xia, C. He, J. Zhang, Y. Liu, C. Wan, C. Fang, C. Guo, W. Yang, and Y. Guang, "Current-driven magnetization switching in a van der Waals ferromagnet Fe<sub>3</sub>GeTe<sub>2</sub>," Sci. Adv. 5, 8904 (2019).
- 14C. Fang, C. H. Wan, C. Y. Guo, C. Feng, X. Wang, Y. W. Xing, M. K. Zhao, J. Dong, G. Q. Yu, Y. G. Zhao, and X. F. Han, "Observation of large anomalous Nernst effect in 2D layered materials Fe<sub>3</sub>GeTe<sub>2</sub>," Appl. Phys. Lett. 115, 212402
- 15T. Liu, J. Peiro, D. K. de Wal, J. C. Leutenantsmeyer, M. H. Guimarães, and B. J. van Wees, "Spin caloritronics in a CrBr<sub>3</sub>-based magnetic van der Waals heterostructure," Phys. Rev. B **101**, 205407 (2020).
- <sup>16</sup>N. Ito, T. Kikkawa, J. Barker, D. Hirobe, Y. Shiomi, and E. Saitoh, "Spin Seebeck effect in the layered ferromagnetic insulators CrSiTe<sub>3</sub> and CrGeTe<sub>3</sub>," Phys. Rev. B **100**, 060402(R) (2019).
- <sup>17</sup>J. Xu, W. A. Phelan, and C. L. Chien, "Large anomalous nernst effect in a van der Waals ferromagnet Fe<sub>3</sub>GeTe<sub>2</sub>," Nano Lett. **19**, 8250 (2019).
- 18E. C. Stoner and E. P. Wohlfarth, "A mechanism of magnetic hysteresis in heterogeneous alloys," Philos. Trans. R. Soc. A 240(826), 599-642 (1948).
- <sup>19</sup>C. Tannous and J. Gieraltowski, "The Stoner-Wohlfarth model of ferromagnetism," Eur. J. Phys. **29**, 475 (2008).
- <sup>20</sup>A. Thiaville, "Extensions of the geometric solution of the two dimensional coherent magnetization rotation model," JMMM 182, 5 (1998).

<sup>22</sup>P. Tang, X. F. Han, and S. Zhang, "Quantum theory of spin-torque driven magnetization switching," Phys. Rev. B 103, 094442 (2021).

 <sup>23</sup> J. L. Lado and J. Fernández-Rossier, "On the origin of magnetic anisotropy in two dimensional CrI<sub>3</sub>," 2D Mater 4, 035002 (2017).
 24 Z. Zhang, J. Shang, C. Jiang, A. Rasmita, W. Gao, and T. Yu, "Direct photolu-

<sup>&</sup>lt;sup>24</sup>Z. Zhang, J. Shang, C. Jiang, A. Rasmita, W. Gao, and T. Yu, "Direct photoluminescence probing of ferromagnetism in monolayer two-dimensional CrBr<sub>3</sub>," Nano Lett. 19, 3138 (2019).